A NOVEL HYBRID $MgFe_2O_4$@UiO-66(Zr)-NH_2 NANOCOMPOSITE WITH ENHANCED PHOTOCATALYTIC ACTIVITY UNDER VISIBLE LIGHT IRRADIATION

Đến tòa soạn 02-03-2021

Vo The Ky
Chemical Engineering Department, Industrial University of Ho Chi Minh City

TÓM TẮT

VẬT LIỆU NANOCOMPOSITE $MgFe_2O_4$@UiO-66(Zr)-NH_2 VỚI HOẠT TÍNH QUANG XÚC TÁC CAO DƯỚI ĐIỀU KIỆN ÁNH SÁNG KHẢ KIẾN

Vật liệu quang xúc tác trên nền khung hữu cơ-kim loại (MOFs) đã nhận được sự quan tâm đáng kể trong những năm gần đây. Trong nghiên cứu này, vật liệu nanocomposite $MgFe_2O_4$@UiO-66(Zr)-NH_2 được tổng hợp bằng phương pháp nhiệt phân dung môi. Cấu trúc và tính chất vật liệu được đặc trưng bằng các phương pháp phân tích, bao gồm hấp phụ-giải hấp N_2, SEM, TEM, FT-IR, XRD, và DRS. Thí nghiệm loại bỏ kháng sinh tetracycline (TC) trong môi trường nước chỉ ra rằng composite $MgFe_2O_4$@UiO-66(Zr)-NH_2 có hiệu suất loại bỏ TC đạt ~ 85% trong 50 phút tiền hấp phụ và 150 phút chiếu xạ bằng ánh sáng khả kiến, cao hơn cả $MgFe_2O_4$ (~42%) và UiO-66(Zr) -NH_2 (~61%). Hiệu quả quang phân hủy được cải thiện trên vật liệu $MgFe_2O_4$@UiO-66(Zr)-NH_2 do sự tách và di cư hiệu quả hơn của lỗ trống và electron giữa hai thành phần bán dẫn trong composite. Ngoài ra, vật liệu nanocomposite $MgFe_2O_4$@UiO-66(Zr)-NH_2 có khả năng tái sinh tốt và độ bền cao sau các lần tái sử dụng.

Từ khóa: *Quang xúc tác, UiO-66(Zr)-NH_2, $MgFe_2O_4$, tetracycline, ánh sáng khả kiến.*

1. INTRODUCTION

Tetracyclines (TCs) are reportedly one of the most extensively-used antibiotics in aquaculture and veterinary medicines [1-3]. Like most antibiotic compounds, tetracycline cannot be adsorbed entirely or transformed inside bodies after utilization.Tetracyclines (TCs) are reportedly one of the most extensively-used antibiotics in aquaculture and veterinary medicines [1-3]. Like most antibiotic compounds, tetracycline cannot be adsorbed entirely or transformed inside bodies after utilization. As a result, a large quantities amount of this antibiotic compound is released into the environment as metabolites. The accumulation of this antibiotic residue and its metabolites in the environment can cause serious harm to the ecological environment as well as human health since they are biologically toxic, stable, and can be transmitted into the food chains[1, 4, 5]. Moreover, these antibiotics residues can cause the development of multi-resistant bacterial strains that can no longer be treated with the presently known drugs [6, 7]. Thus, the removal of antibiotic residues from the environment has received great attention. Many techniques have been developed to eliminate antibiotic residues, such as ion exchange, anaerobic digestion, ozonation, electrochemical oxidation, adsorption, and semiconductor-based photocatalytic degradation, etc. [3, 8-12]. Among them, photocatalysis has been considered as one of the promising approaches for degrading antibiotic residues because of its cost-effectiveness, high efficiency, and eco-friendly technique along with ease of operation [4, 13-

15]. Nevertheless, most photocatalysts are difficult to recycle and constantly secondary pollutants in the environment [5, 12]. To solve these problems, the development of magnetic photocatalysts that can be easily recovered is considered a promising solution. Among the synthesized magnetic materials, magnesium ferrite $MgFe_2O_4$, a type of spinel ferrite (AFe_2O_4), has been gained considerable attention because it possesses both photocatalytic and magnetic properties [1, 16-19]. However, the use of ferrite materials is often limited because they exhibited low adsorptive performance towards pollutants caused by their low surface area and pore volume.

In this work, magnetic framework composite $MgFe_2O_4$@UiO-66(Zr)-NH_2 was effectively fabricated via hydrothermal approach. The obtained samples were characterized by field-emission scanning electron microscopy (FE-SEM), high-resolution transmission electron microscopy (HR-TEM), powder X-ray diffraction (PXRD), diffuse reflectance spectroscopy (DRS), and N_2 adsorption–desorption. The fabricated $MgFe_2O_4$@UiO-66(Zr)-NH_2 composite were then applied for removal of tetracycline antibiotic under visible light irradiation. It was observed that the combination UiO-66(Zr)-NH_2 framework and $MgFe_2O_4$ together to a composite improved both the adsorption ability and photocatalytic activity due to a synergistic effect.

2. EXPERIMENTAL

2.1. Materials

Magnesium nitrate $Mg(NO_3)_2.6H_2O$ (Aldrich, 98%) , iron nitrate ($Fe(NO_3)_3$. $9H_2O$ (Aldrich, 99%), citric acid (Aldrich, 97%), Zirconium chloride ($ZrCl_4$, Aldrich, 98%) and 2-amino terephthalic acid (H_2N-BDC, Aldrich, 97%), and tetracycline ($C_{22}H_{24}N_2O_8$, Aldrich, 99%) were purchased from Aldrich Sigma company. N, N-demethylformamide (DMF, 98%, Ethanol (99%) were supported Shanghai Makclin Biochemical Co., Ltd (Shanghai, China).

2.2. Synthesis of $MgFe_2O_4$ ferrite

Magnesium ferrite, $MgFe_2O_4$, was prepared employing the sol-gel approach followed the previous procedure with a slight modification[20]. Typically, a solution was prepared by dissolving 3 mmol $Mg(NO_3)_2.6H_2O$ and 6 mmol $Fe(NO_3)_3$. $9H_2O$ in deionized water. To the resultant solution, 25 mmol citric acid was introduced and stirred until a thick gel was produced. The resulting gel was then calcined at 400 ^oC to obtain the powder, followed by ground in a mortar and pestle. Finally, the produced powder was calcined at 650 ^oC for 8h to yield the $MgFe_2O_4$ ferrite nanoparticles.

2.3. Synthesis of hybrid $MgFe_2O_4$@UiO-66(Zr)-NH_2 nanocomposite

Magnetic framework composite $MgFe_2O_4$@UiO-66(Zr)-NH_2 was simply prepared by solvothermal method. Typically, 0.3 g of $MgFe_2O_4$ powder was dispersed in 30 ml DMF with constant stirring. To the resultant mixture, 3g of $ZrCl_4$ and 3g of H_2N-BDC were added. The mixture was sonicated for 5 min before being transferring into a Teflon-lined autoclave (100 ml) and sealed in a stainless steel vessel. The reactor was kept at 130 ^oC for 24 h in a convection oven, then cooled down to room temperature. The resulting mixture was centrifuged to collect the solid product, which was then washed with DMF (6 h) and ethanol (6 h) to remove the remaining reactants. The resulting solid was dried at 70 ^oC for 12 h, and then degassed at 120 ^oC under vacuum (10^{-2} kPa) for 8h before using. The produced magnetic framework composite was labelled as $MgFe_2O_4$@UiO-66(Zr)-NH_2.

2.4. Analyses

X-ray diffraction (XRD) analysis was conducted on MAC-18XHF (Rigaku, Japan) using Cu-K_α radiation. Scanning electron microscopy (SEM) evaluation was performed using a field emission scanning electron microscope (FESEM) (Leo-Supra 55, Carl Zeiss STM, Germany). The N_2 sorption isotherms at 77 K were obtained utilizing Micrometrics instruments (BELSORP-max, BEL, Japan). The surface area was estimated

employing the multiple-point Brunauer–Emmett–Teller (BET) method in the pressure range of $0.05 < P/P_0 < 0.20$. The BET surface area was calculated by fitting the isotherm data in the 0–0.1 P/P_0 range.

2.5. Adsorption-photocatalytic degradation experiment

Adsorption-photocatalytic degradation of tetracycline antibiotic was performed in the photochemical reaction cell, assembled with a 500 W Xe lamp and an optical filter ($\lambda > 420$ nm) to simulate visible light. For each run, 50 ml of tetracycline solution (30 ppm) was introduced into the reactor. Then 40 ± 5 mg of material ($MgFe_2O_4$, UiO-66(Zr)-NH_2, or $MgFe_2O_4$/UiO-66(Zr)-NH_2) was added in the solution and magnetically stirred for 50 min in the dark. Next, the mixture was irradiated by the visible-light with stirring. About 5 ml the reaction mixture was taken out after an interval time and centrifuged to collect the clear solution, of which the content of tetracycline was measured using an UV-visible spectrophotometry (Optizen POP, Mecasys, Korea).

3. RESULTS AND DISCUSSION

3.1. Characterization

Fig. 1 shows SEM images of the bare $MgFe_2O_4$ ferrite, UiO-66(Zr)-NH_2 and $MgFe_2O_4$@UiO-66(Zr)-NH_2 composite samples. As shown, the produced $MgFe_2O_4$ exhibited nanospheres with sizes ranged 20 nm~50 nm. The SEM image reveal the produced $MgFe_2O_4$@UiO-66(Zr)-NH_2 composites with highly agglomerated nanoparticles. TEM analysis indicated that the composite structure has been formed between $MgFe_2O_4$ and UiO-66(Zr)-NH_2.

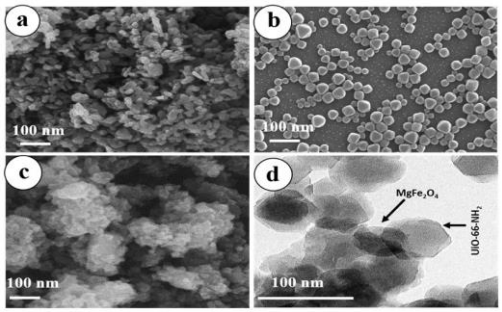

Fig. 1 SEM analysis of (a) $MgFe_2O_4$, (b) UiO-66(Zr)-NH_2, (c)$MgFe_2O_4$@UiO-66-NH_2, and (d) TEM analysis of $MgFe_2O_4$@UiO-66-NH_2

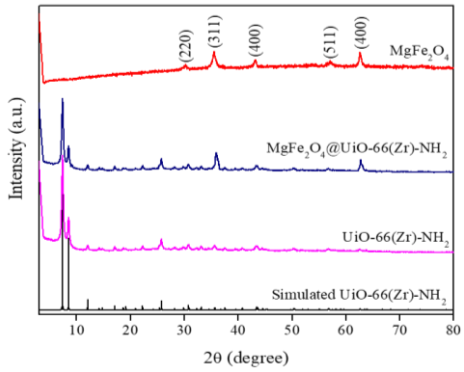

Fig. 2. XRD analysis of $MgFe_2O_4$, UiO-66(Zr)-NH_2, and $MgFe_2O_4$@UiO-66-NH_2 sample

The crystallography analyses of the prepared samples were performed and presented in Figure 2. The XRD pattern of pure $MgFe_2O_4$ ferrite showed the predominant peaks at 2θ = 35.5 ° and 62.6 °, corresponding to the diffraction plane of (311) and (400) of $MgFe_2O_4$ crystal [21, 22]. The prepared amino-functionalized UiO-66(Zr) exhibited a similar XRD pattern with that previously reported in the literatures [23-25], and with the simulated one of UiO-66(Zr) framework. XRD pattern of the produced $MgFe_2O_4$@UiO-66-NH_2 showed both peak diffraction of the ferrite and UiO-66(Zr)-NH_2. As can be seen that the peak intensities of UiO-66(Zr)-NH_2 considerably decreased on the XRD patterns of $MgFe_2O_4$@UiO-66-NH_2 compared to those of the pure MOF, implying the formation of the hybrid composite structure.

Figure 3 shows nitrogen adsorption-desorption for all fabricated samples. It can be seen that the N_2 -uptake capacity of the prepared magnetic framework was lower than that of MOF, suggesting the micropores are occupied and blocked by incorporating of the ferrites. Furthermore, the increase N_2-uptake capacity and presence of clear hysteresis loops at high P/P_o value on the hybrid composites are attributed to the formation of new pore structures in the resulting $MgFe_2O_4$@UiO-66(Zr)-NH_2 composite[23, 26]. The calculated BET surface area and pore volume of the prepared materials are shown in Table 1. As shown, the prepared $MgFe_2O_4$@UiO-66(Zr)-NH_2 had surface area and pore volume of 138

m^2 g^{-1} and 0.32 cm ^{3} g^{-1}, respectively, which were greater than those of bare $MgFe_2O_4$.

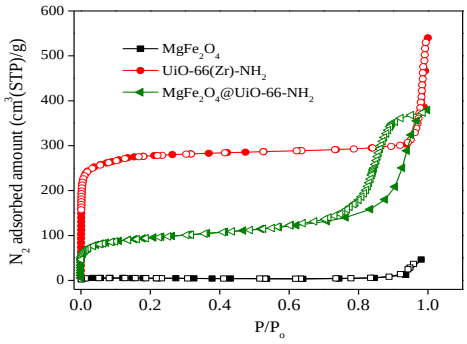

Fig.3 N_2 adsorption –desorption of the prepared samples

Table 1 Textural properties of the synthesized samples

Sample	**S_{BET} , m^2 g^{-1}**	**Pore volume, cm^3 g^{-1}**
$MgFe_2O_4$	36	0.11
UiO-66(Zr)-NH_2	987	0.75
$MgFe_2O_4$@UiO-66(Zr)-NH_2	138	0.32

Figure 4 shows the UV-vis diffuse reflectance spectrum of $MgFe_2O_4$, and $MgFe_2O_4$@UiO-66(Zr)-NH_2. As shown, the DRS shows the absorbance in the range 450-600 nm range, showing their responses in the visible spectrum. By employing the Tauc's plot method, the estimated band gap energy (E_g) value of $MgFe_2O_4$ and $MgFe_2O_4$@UiO-66(Zr)-NH_2 composite were ~ 2.2 eV, and ~2.5 eV, respectively, suggesting their suitable potency to capture the visible light.

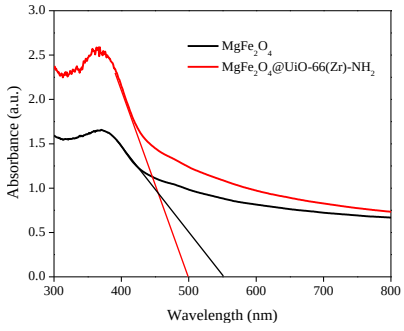

Fig. 4 UV-vis diffuse reflectance spectra of the pure $MgFe_2O_4$, and $MgFe_2O_4$@UiO-66(Zr)-NH_2

3.2. Adsorption-photocatalytic degradation of tetracycline

Fig. 5(a) shows the UV-vis spectrum of tetracycline as a function of sampling time of $MgFe_2O_4$@UiO-66-NH_2, and Fig. 5(b) shows the removal efficiency of tetracycline over antibiotic of the fabricated $MgFe_2O_4$ ferrite, UiO-66(Zr)-NH_2, or $MgFe_2O_4$@UiO-66(Zr)-NH_2 composite. As shown, TC was strongly adsorbed onto the bare UiO-66(Zr)-NH_2 for the first 50 min in the dark (~43%), it then slowly decreased when the solution was irradiated. This suggests that TC was predominantly removed from the solution by the adsorption process of UiO-66(Zr)-NH_2 framework. Meanwhile the photocatalytic degradation of UiO-66(Zr)-NH_2 was ineffective owing to the poor charge separation and transfer from the excited ligands to the Zr-O clusters inside MOF[8, 14, 27]. For bare magnesium ferrite $MgFe_2O_4$, there were a small amount of TC removed (~8 %) during the pre-adsorption stage. The removal yield of tetracycline then further increased up to ~ 42% when the solution was irradiated by the visible light for 150 min. This obtained result is consistent with the previous observation that $MgFe_2O_4$ ferrite adsorbs visible light to generate electron-hole pairs, which directly caused the oxidation of the organic pollutants [1, 16, 28].

As revealed, the produced magnetic framework composite $MgFe_2O_4$@UiO-66(Zr)-NH_2 exhibited significantly improved removal efficiency of TC compared to the formers. At the pre-adsorption stage, the amount of TC captured onto the composite samples were enhanced mainly caused by the presence of MOF in the composite. Then, the removal of TC was accelerated by the photodegradation under visible light irradiation. After 150-min exposure to the light, the total removal efficiency of TC over the $MgFe_2O_4$@UiO-66(Zr)-NH_2 was approximately 85 %. Such improvements of photocatalytic activities on the hybrid $MgFe_2O_4$@UiO-66(Zr)-NH_2 composites 'surface could be resulted from a synergistic effect of the combination of two

different types of semiconductors, through which separation and immigration processes of the photo-generated charge carriers were promoted. This was further improved by making a comparison with a physically mixed mixture contained the same MOF/ferrite ratio, which showed a far lower photodegradation of TC under the same conditions.

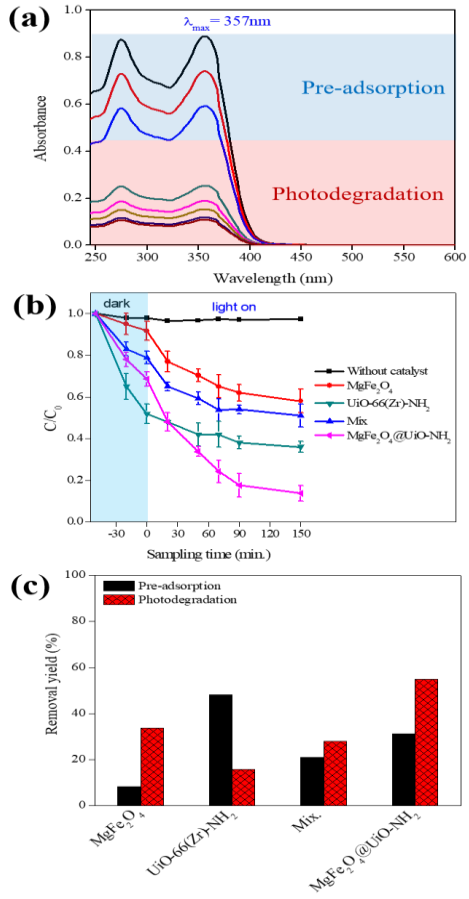

Fig. 5 The removal of TC using different materials: (a) UV-vis spectrum of TC, (b) Removal efficiency of TC, and (d) Pre-adsorption and photodegradation of TC over different materials

The photo-generated species including $\cdot O_2^-$, $\cdot OH$, and h^+ are reportedly responsible for the photocatalyzed degradation of catalysts [1, 4, 8, 16, 29]. Jiang et al. [1] reported that the photocatalytic degradation of TC over a rod-in-tube nanostructure of $MgFe_2O_4$ ferrite was primarily driven by photogenerated holes and hydroxyl radicals. However, the maximum removal efficiency of TC over the rod-in-tube $MgFe_2O_4$ only reached ~64% after 120-min visible light irradiation[1], which was far lower than that of the present hybrid $MgFe_2O_4$@UiO-66(Zr)-NH_2 composite.

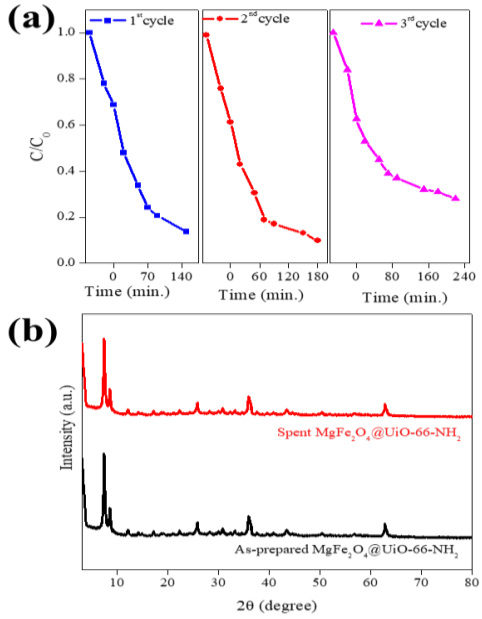

Fig. 6 (a) Regenerability experiment, and (b) XRD pattern of the as-prepared and spent catalyst

3.3. Reusability of $MgFe_2O_4$@UiO-66 (Zr)-NH_2

For regenerability experiment, the used catalyst was first effectively separated from the solution by centrifuged. Next, the spent material was regenerated by washing with methanol several times and dried at 110 ºC for 4h under vacuum. The catalyst was then used for the next adsorption-photocatalytic degradation experiment. **Fig. 6(a)** shows three successive renewability experiments of the fabricated $MgFe_2O_4$@UiO-66(Zr)-NH_2 catalyst. As shown, the total removal efficiency of antibiotic compound in the second run was ~81 % achieved after 180 min. After three cycles, the total removal yield remained ~72.5% within 240 min. **Fig. 6(b)** shows the XRD of the spent material, revealing their structure was unchanged after 4 cycles.

4. CONCLUSIONS

The $MgFe_2O_4$@UiO-66 (Zr)-NH_2 nanocomposite was successfully synthesized and characterized. The prepared

$MgFe_2O_4$@UiO-66 (Zr)-NH_2 had surface area and pore volume of 138 m^2 g^{-1} and 0.32 cm^3 g^{-1}, respectively, which was greater than that of bare ferrite. The removal of TC over $MgFe_2O_4$@UiO-66(Zr)-NH_2 was controlled by the pre-adsorption and photodegradation processes. The prepared $MgFe_2O_4$@UiO-66(Zr)-NH_2 exhibited an optimal synergy effect between two semiconductors resulted in its highest total TC removal yield of ~85 % after 50-min pre-adsorption and 150-min visible light irradiation, which was ~2.0 and ~1.4 times greater than that over bare $MgFe_2O_4$ and UiO-66(Zr)-NH_2, respectively. The prepared MFO@UNH exhibited good reusability after several recycles. These suggest that the fabricated $MgFe_2O_4$@UiO-66(Zr)-NH_2 composite can be a promising material for the removal of antibiotics from wastewater.

REFERENCES

1. Jiang, J., et al., *Rod-in-tube nanostructure of MgFe2O4: electrospinning synthesis and photocatalytic activities of tetracycline.* New Journal of Chemistry, 2016. **40**(1): p. 538-544.

2. Palominos, R.A., et al., *Photocatalytic oxidation of the antibiotic tetracycline on TiO2 and ZnO suspensions.* Catalysis Today, 2009. **144**(1): p. 100-105.

3. Liu, S., et al., *The degradation of tetracycline in a photo-electro-Fenton system.* Chemical Engineering Journal, 2013. **231**: p. 441-448.

4. Wu, S., et al., *Visible light photocatalytic degradation of tetracycline over TiO2.* Chemical Engineering Journal, 2020. **382**: p. 122842.

5. Li, J., et al., *Eggshell membrane-derived MgFe2O4 for pharmaceutical antibiotics removal and recovery from water.* Chemical Engineering Research and Design, 2017. **126**: p. 123-133.

6. Addamo, M., et al., *Removal of drugs in aqueous systems by photoassisted degradation.* Journal of Applied Electrochemistry, 2005. **35**(7): p. 765-774.

7. Zhu, X.-D., et al., *Photocatalytic degradation of tetracycline in aqueous solution by nanosized TiO2.* Chemosphere, 2013. **92**(8): p. 925-932.

8. Bibi, R., et al., *Hybrid BiOBr/UiO-66-NH2 composite with enhanced visible-light driven photocatalytic activity toward RhB dye degradation.* RSC Advances, 2018. **8**(4): p. 2048-2058.

9. Wei, Z., J. Liu, and W. Shangguan, *A review on photocatalysis in antibiotic wastewater: Pollutant degradation and hydrogen production.* Chinese Journal of Catalysis, 2020. **41**(10): p. 1440-1450.

10. Eswar, N.K., P.C. Ramamurthy, and G. Madras, *Novel synergistic photocatalytic degradation of antibiotics and bacteria using V–N doped TiO2 under visible light: the state of nitrogen in V-doped TiO2.* New Journal of Chemistry, 2016. **40**(4): p. 3464-3475.

11. Abdurahman, M.H., A.Z. Abdullah, and N.F. Shoparwe, *A comprehensive review on sonocatalytic, photocatalytic, and sonophotocatalytic processes for the degradation of antibiotics in water: Synergistic mechanism and degradation pathway.* Chemical Engineering Journal, 2020: p. 127412.

12. Li, D. and W. Shi, *Recent developments in visible-light photocatalytic degradation of antibiotics.* Chinese Journal of Catalysis, 2016. **37**(6): p. 792-799.

13. Shen, L., et al., *CdS-decorated UiO–66(NH2) nanocomposites fabricated by a facile photodeposition process: an efficient and stable visible-light-driven photocatalyst for selective oxidation of alcohols.* Journal of Materials Chemistry A, 2013. **1**(37): p. 11473-11482.

14. Shen, L., et al., *Electronic effects of ligand substitution on metal–organic framework photocatalysts: the case study of UiO-66.* Physical Chemistry Chemical Physics, 2015. **17**(1): p. 117-121.

15. Vo, T.K. and J. Kim, *Facile synthesis of mesoporous Cr2O3 microspheres by spray pyrolysis and their photocatalytic activity:*

Effects of surfactant and pyrolysis temperature. Korean Journal of Chemical Engineering, 2020. **37**(3): p. 571-575.
16. Shahid, M., et al., *Photocatalytic degradation of methylene blue on magnetically separable MgFe2O4 under visible light irradiation.* Materials Chemistry and Physics, 2013. **139**(2): p. 566-571.
17. Shen, Y., et al., *One-pot synthesis of MgFe2O4 nanospheres by solvothermal method.* Materials Letters, 2013. **96**: p. 85-88.
18. Tran, C.V., et al., *Effective Removal of Pb(II) from Aqueous Media by a New Design of Cu–Mg Binary Ferrite.* ACS Omega, 2020. **5**(13): p. 7298-7306.
19. Guijarro, N., et al., *Evaluating spinel ferrites MFe2O4 (M = Cu, Mg, Zn) as photoanodes for solar water oxidation: prospects and limitations.* Sustainable Energy & Fuels, 2018. **2**(1): p. 103-117.
20. Naik, M.Z. and A.V. Salker, *Tailoring the super-paramagnetic nature of MgFe2O4 nanoparticles by In3+ incorporation.* Materials Science and Engineering: B, 2016. **211**: p. 37-44.
21. Loganathan, A. and K. Kumar, *Effects on structural, optical, and magnetic properties of pure and Sr-substituted MgFe2O4 nanoparticles at different calcination temperatures.* Applied Nanoscience, 2016. **6**(5): p. 629-639.
22. Heidari, P. and S.M. Masoudpanah, *Structural and magnetic properties of MgFe2O4 powders synthesized by solution combustion method: the effect of fuel type.* Journal of Materials Research and Technology, 2020. **9**(3): p. 4469-4475.
23. Vo, T.K., et al., *Microwave-assisted continuous-flow synthesis of mixed-ligand UiO-66(Zr) frameworks and their application to toluene adsorption.* Journal of Industrial and Engineering Chemistry, 2020. **86**: p. 178-185.
24. Fu, Y., et al., *Temperature modulation of defects in NH2-UiO-66(Zr) for photocatalytic CO2 reduction.* RSC Advances, 2019. **9**(65): p. 37733-37738.
25. Shen, L., et al., *Multifunctional NH2-mediated zirconium metal–organic framework as an efficient visible-light-driven photocatalyst for selective oxidation of alcohols and reduction of aqueous Cr(vi).* Dalton Transactions, 2013. **42**(37): p. 13649-13657.
26. Vo, T.K., et al., *Formation of structural defects within UiO-66(Zr)-(OH)2 framework for enhanced CO2 adsorption using a microwave-assisted continuous-flow tubular reactor.* Microporous and Mesoporous Materials, 2021. **312**: p. 110746.
27. Sun, D., et al., *Introduction of a mediator for enhancing photocatalytic performance via post-synthetic metal exchange in metal–organic frameworks (MOFs).* Chemical Communications, 2015. **51**(11): p. 2056-2059.
28. Ji, H., et al., *Magnetic g-C3N4/NiFe2O4 hybrids with enhanced photocatalytic activity.* RSC Advances, 2015. **5**(71): p. 57960-57967.
29. Bagwasi, S., et al., *Synthesis, characterization and application of bismuth and boron Co-doped TiO2: A visible light active photocatalyst.* Chemical Engineering Journal, 2013. **217**: p. 108-118.